Journal of Applied Polymer Science

Electrochemical behavior of multifunctional graphene-polyimide nanocomposite film in two different electrolyte solutions

Patricia Azuka Okafor, Brenton Huxel, Jude O. Iroh
Material Science and Engineering Program, School of Mechanical and Materials Engineering, University of Cincinnati, Cincinnati, Ohio 45221
Correspondence to: J. O. Iroh (E-mail: irohj@ucmail.uc.edu)

ABSTRACT: The effect of solvent on specific capacitance, bulk resistance, and charge/discharge capacity of graphene/polyimide composite films is studied by electrochemical methods. Composite films are synthesized by *in situ* condensation polymerization of poly (amic acid) in the presence of 50 wt % partly exfoliated graphene sheets followed by thermal curing at 250°C. Raman spectrum of the exfoliated graphene sheets show an increase in the ratio of I_D to I_G peak intensities from 0.167 to 0.222, suggesting increased defects in graphene basal planes. Electrochemical measurements carried out by using 0.4*M* potassium hexafluorophosphate (KPF_6) dissolved in propylene carbonate and *N*-methylpyrrolidone at 25°C show that the composite system exhibits both pseudocapacitance and supercapacitance behaviors, with an average capacitance of 40 and 36.5 F g^{-1}, respectively. Bulk resistance of the composite obtained by using KPF_6–propylene carbonate electrolyte solution is 300% lower than that obtained in KPF_6–*N*-methylpyrrolidone solution, with a fairly stable specific capacity of 85 μAhr g^{-1}, with 80% retention observed after 30 charge–discharge cycles. Fourier transform infrared spectroscopy measurements show shifts in the cyclic imide carbonyl peak from 1778 to 1774 cm^{-1}, which suggests that some form of interaction exists between the graphene and polyimide. © 2015 Wiley Periodicals, Inc. J. Appl. Polym. Sci. **2015**, *132*, 42673.

KEYWORDS: blends; composites; fullerenes; graphene; nanoparticles; nanotubes; nanowires and nanocrystals

Received 11 February 2015; accepted 28 June 2015
DOI: 10.1002/app.42673

INTRODUCTION

Over the past few decades, the demand for sustainable green energy has increased because of the depletion and environmental concern of continued use of fossil fuels. Supercapacitors represent an alternative source of energy for portable electronics and automobile applications because of their high specific power and extended life-time. They store electrical energy through double layer charging, faradaic processes, or a combination of both. The amount of energy stored is small and can be delivered instantaneously, making supercapacitors capable of providing pulsed high power rather than high amount of energy. The quest for cheaper, portable, and more durable electrode material for such devices have led to the discovery of graphene-based polymer nanocomposite materials. The interest in conductive composite materials as alternative material in such applications is due to their availability, low cost, and environmental friendliness.[1–5]

Graphene/polyimide composites are being explored for use as electrode materials in electronic devices, fabricated field-effect transistors, and ultrasensitive chemical sensors such as pH sensors, gas sensors, and biosensors because of their environmental stability, low density, and environmental friendliness.[4] The superior electrical conductivity and the extremely large surface area of graphene and the excellent mechanical and thermal stability of polyimide makes this composite material a strong contender for use in energy storage, supercapacitors, fuel cell, solar energy, electronic display devices, and biosensors.[6]

Graphene is a single-layered sp^2-bonded two-dimensional structure consisting of six fused membered carbon rings with outstanding electronic transport properties and high electrocatalytic activities. It has many unique properties, such as high surface area $\sim 2.965 \times 10^6$ m^2 kg^{-1}, excellent conductivity ~3000–5000 W m^{-1} K^{-1}, good optical transparency ~97.7%, and high charge carrier mobility at room temperature ~10,000 cm^2 V^{-1} S^{-1}. Charge carriers of graphene exhibit great intrinsic mobility, have zero effective mass, and can travel for micrometers without scattering at room temperature. Graphene sustains current densities six orders of magnitude higher than that of copper, and hence, it has a promising application in energy storage.[7] Polyimide, on the other hand, is considered a superior engineering plastic because of its thermal stability >400°C, high glass-transition temperature >300°C, high tensile strength, low creep, excellent radiation shielding capability, flexibility, and low color. It has interesting

applications in the field of aeronautics and electronics because of its durability and resistance against ultaviolet radiation and low dielectric constants. Nanoparticles like graphene are added to polyimide to improve its mechanical and physical properties so as to give them the desired property for other advanced applications.[8,9] Dispersion is key in achieving high-quality homogeneous graphene–polymer composites. Graphene sheets have a high tendency to agglomerate because of the strong van der Waal forces that exist between them. Agglomeration results in poor physical and chemical properties of composite materials.[10] To address this, exfoliation of graphene sheets is carried out to enhance filler–matrix interaction, thereby minimizing agglomeration, and improve properties of the composite material. Exfoliated graphene in graphene–polyimide composites show enhanced properties because of the synergistic combination of high specific surface area and strong nanofiller–matrix adhesion.[11,12]

In this article, we report our study of the electrochemical behavior of graphene–polyimide composite films using potassium hexafluorophosphate (KPF_6) electrolyte dissolved in two different solvents—propylene carbonate (PC) and *N*-methylpyrrolidone (NMP). The choice of electrolyte is due to the wide electrochemical window of potassium ions (K^+ has a standard potential of −2.92V vs. SHE), which is slighly less than that of $Li^+ \sim -3.04$ V, high mobility, and chemical diffusion coefficient of potassium ions K^+ due to its small stokes radius in electrolyte solution.[13] The choice of solvents is due to the high dielectric constants of PC ∼ 64.92 and NMP ∼ 33, which allows for easy dissolution of electrolyte, low viscosity (PC ∼ 2.53 cP and NMP ∼ 1.65 cP) so that facile ion transport can occur, moderate dipole moments (PC ∼ 4.81 and NMP ∼ 4.1), which enhances ion–dipole interactions, and a wide potential range (PC ∼ −3.5V to +3.5V and NMP ∼ −4.0V to +1.2V).[14] PC, a dipolar aprotic solvent commonly used in lithium ion batteries is one of the most widely used solvent because of its mild solvation of electrolyte ions. However, NMP on the other hand, is a polar aprotic solvent with good solvency that strongly coordinates to cations with its oxygen atom because it is a hard base. The use of NMP in electrochemical systems is limited because of its hard solvation of alkali metal ions, which affects electrochemical properties.[13] In this study, a comparison of electrochemical behavior of graphene–polyimide composite film tested by using both electrolyte–solvent systems is made. The electrochemical tests performed includes cyclic voltammetry (CV), electrochemical impedance spectroscopy (EIS), and cyclic charge–discharge (CCD) tests. The composites structure and morphology were studied by using Raman spectroscopy, Fourier transform infrared spectroscopy (FTIR), and scanning electron miscroscopy (SEM).

EXPERIMENTAL

Synthesis and Preparation of Graphene–Polyimide Films

The reagents used in this study are as follows: nano graphene sheets (98.48% purity) with thickness 50–100 nm and length 7 μm purchased from Angstron Materials (Dayton, OH). Twelve grams of graphene powder was dissolved in 100 mL NMP and sonicated at room temperature for 2 h to break up the multi-stacked sheets. After sonication, the exfoliated graphene was filtered out and washed several times with distilled water to get rid of the solvent. It was then dried in the oven at low heat for 6 h. Pyromellitic dianhydride (99% purity), 4,4-oxydianiline (ODA), and NMP (99% purity) were purchased from Sigma-Aldrich (St. Louis, MO). For composite synthesis, 5.2 g of ODA was added to a round-bottom flask containing 100 mL of NMP followed by steady mechanical stirring for 30 min. 10.8 g (50 wt %) of the mechanically exfoliated nanographene powder was added to the mixture in a gradual steady manner, and the stirring speed was increased. After 8 h of stirring, 5.6 g of pyromellitic dianhydride was added to the mixture and mechanical stirring continued for another 12 h while the temperature was maintained at 10°C by means of a constant temperature bath. The experiment was carried out in an inert atmosphere with a steady purge of nitrogen gas. Free-standing films are prepared by the traditional solution casting method. The suspension was cast onto a clean glass plate and thermally imidized in a stepwise manner in a vacuum oven at 120°C for 2 h, 200°C for 1 h, and 250°C for 1 h under vacuum.

Characterization

Thermo-Scientific NXR 9560 FT-Raman spectroscopy with an InGaAs detector and laser beam wavelength of 785 nm and laser power of 200 mV was used to study the structure of graphene sheets. Thermo Scientific Nicolet 6700 FTIR (diamond small orbit module) was used to study the chemical composition and structure of the composites. Composite film morphology was studied by using Phillips XL30 ESEM FEG environmental SEM. A split flat cell electrode (shown in Figure 1) consisting of positive and negative terminals (working and counter electrodes) and an inner surface diameter of 0.725 cm^2 was used for electrochemical measurements. KPF_6 (98% purity) and PC (99% purity) purchased from Sigma-Aldrich was used to perform the electrochemical tests.

0.4*M* KPF_6 electrolyte was dissolved in 10 mL of PC and NMP solvents separately and sonicated for 30 min to allow for homogenity. The composite film was then cut into two small circlular pieces with a surface area 0.625 cm^2 and mass of 0.0012 g and assembled into the cell separated by a polypropylene permeable membrane. 1.5 mL of the electrolytic solution was added in a dropwise manner into the sandwiched electrode and the cell securely fastened. CV was done by using an AC voltage range of 0–3 V and −0.2 to 1 V and scan rates ranging from 5 to 100 mV s^{-1} for both electrolyte–solvent systems. EIS measurement was carried out by using the same electrochemical cell setup described earlier, with a low sinusoidal amplitude voltage of 10 mV s rms, an initial frequency of 10 MHz, and a final frequency of 0.01 Hz. CCD test was carried out by using an alternating current in the voltage range of 0–1 V, a maximum current of 1.2×10^{-5} A, and a maximum charge and discharge time of 1 min. The electrochemical tests were performed by using the Gamry 9600 Instrument.

RESULTS AND DISCUSSION

Morphology and Composite Film Structure

Figure 2(a,b) shows the environmental SEM images of pristine graphene nanosheets and graphene sheets dispersed in the polyimide matrix. The 2D structure of the sheets are aligned and

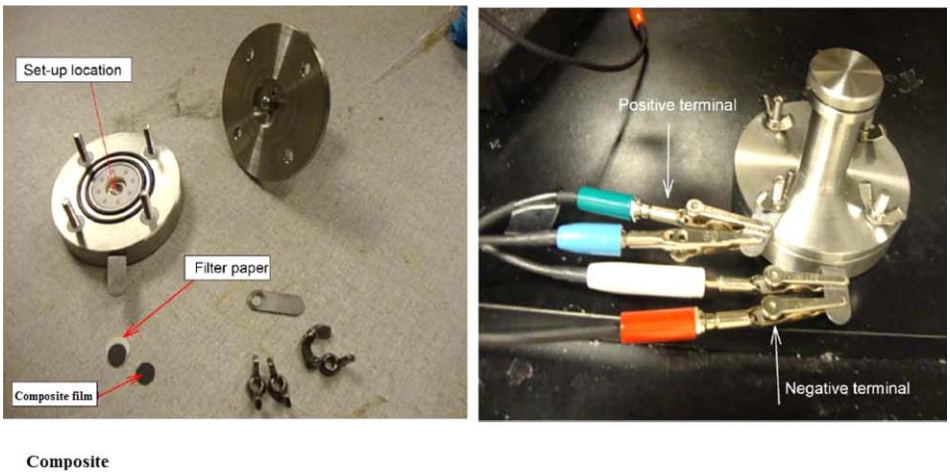

Figure 1. Split flat cell electrode set-up used for electrochemical tests. [Color figure can be viewed in the online issue, which is available at wileyonlinelibrary.com.]

stacked in the same direction within the matrix. The unidirectional alignment of the fillers could be due to interaction between imide functional groups and sites within graphene galleries improving interfacial properties. The stacking of the sheets creates tortuous microporous pathways within the bulk of the composite. Raman spectroscopy is used to study the structure of the exfoliated and pristine graphene sheets. Raman spectroscopy is a non-destructive tool widely used to characterize carbon products especially because conjugated and carbon–carbon double bonds leads to high Raman intensities. Highly ordered graphite has a couple of Raman-active bands, which includes the in-phase vibration of the graphitic lattice (G band) and the disorder band caused by the graphite edges (D band) and a secondary 2D band.[15] The D peak is usually absent in perfect graphite and only becomes prominent in the presence of imperfections.[16] Figure 3(a,b) shows Raman Spectra for pristine graphene sheets and exfoliated graphene sheets, respectively. For both systems, all characteristic graphitic D, G, and 2D peaks are well distinguished. The D peak observed at 1356 cm^{-1} corresponds to κ-point photons of A_{1g} symmetry, G peak observed at 1574 cm^{-1} corresponds to the in-bond plane stretching of sp^2 carbon bonds, and 2D peak at 2746 cm^{-1} corresponds to second-order overtone of a different in-plane vibration. Peak positions shift to lower Raman bands in the partly exfoliated graphene spectrum, with the D peak observed at 1207 cm^{-1}, the G peak observed at 1419 cm^{-1}, and the 2D peak observed at 2630 cm^{-1}. Typically, as layer thickness increases, the G peak position shifts to lower wavenumbers representing softening of the bonds.[17] The shift in G peak to lower wavenumbers is due to re-assembling of layers as soon as applied force is removed due to strong van der Waal force of attraction. The size and intensity of the D peak suggests the presence of higher-level defects, which is proven by the presence of additional peaks at D′ (1460 cm^{-1}) and D + G at (2732 cm^{-1}) shown in Figure 3(b). Quantity of graphitization or defective disorder is measured by the ratios of the D to G bands (I_D/I_G).[18] The I_D/I_G ratio increased from 0.167 in the pristine graphite to 0.222 in the exfoliated graphene. This is due to increase in disordered structure due to mechanical exfoliation.[19]

Figure 4(a,b) shows FTIR spectra for a neat polyimide matrix and graphene–polyimide composite film. The FTIR peak assignments and wave numbers are shown in Table I.

Symmetric and asymmetric stretchings of the imide carbonyl bond occur at 1778 and 1714 cm^{-1} in neat polyimide but shifted to lower and higher wavenumbers of 1774 and 1716 cm^{-1}, respectively, in the composite. Shifts in wavenumber for polyimide carbonyl is due

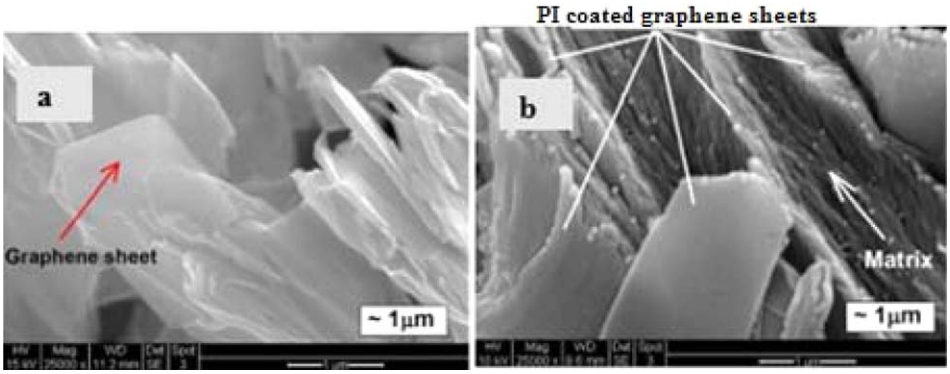

Figure 2. SEM image of (a) graphene sheet and (b) graphene–polyimide composite.[6] [Color figure can be viewed in the online issue, which is available at wileyonlinelibrary.com.]

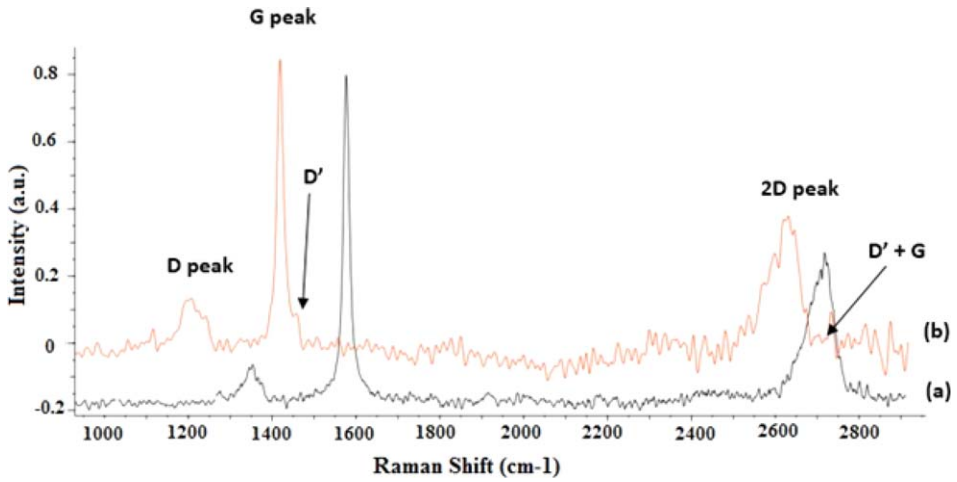

Figure 3. Raman spectra of (a) pristine graphene sheets and (b) partly exfoliated graphene sheets. [Color figure can be viewed in the online issue, which is available at wileyonlinelibrary.com.]

to molecular interactions between the imide carbonyl group and the highly reactive graphitic edges, yielding a strong homogeneous composite system with highly enhanced mechanical properties. Longun and Iroh[6] reported up to 500,000% increase in the rubbery plateau region storage modulus because of the interaction and the pronounced stiffening effect of hard graphene fillers in a polyimide matrix. The broad base of the carbonyl peak at 1716 cm^{-1} in the composite is due to overlapping of the C═C peak of graphene at 1656 cm^{-1}, which further confirms the synergistic combination of the matrix and filler. There is, however, no noticeable shift in the —C—N—C— peak wavenumber for both systems. Decrease in peak intensity observed in the composite material is due to restriction of polyimide chain to chain contacts because of the presence of a filler phase. The extent of imidization of polyimide cured at different curing temperatures was calculated by using eq. (1):

$$\mathrm{EOI}(\alpha) = \frac{H_{\mathrm{imide}}/H_{\mathrm{benzene}}}{H_{\mathrm{imide\ 100}\%}/H_{\mathrm{benzene\ 100}\%}} \quad (1)$$

The imide group absorption intensity is normalized using the benzene absorption band at 1496 cm^{-1}, and the peak size at 1370 cm^{-1} is used to track the extent of imidization.[20] The results are summarized in Table II.

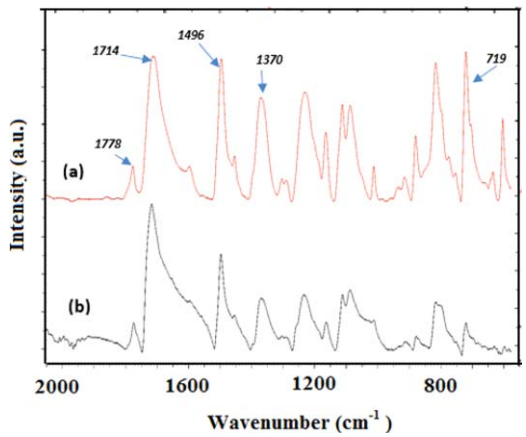

Figure 4. FTIR spectrum of (a) neat polyimide and (b) 50 wt % graphene/polyimide composite system. [Color figure can be viewed in the online issue, which is available at wileyonlinelibrary.com.]

As expected, the EOI increased with increase in curing temperature and reaches a maximum of 79.11% at 250°C. The high surface area of graphene provides more active sites for dehydration and cyclization reactions during the imidization process.[20]

Electrochemical Measurements

Figure 5(a–c) shows cyclic voltammogram for graphene/polyimide composites tested in KPF_6-PC electrolyte solution using scan rates of 5, 15, and 25 mV s^{-1} and voltage range of 0–3 V. Magnitude of current obtained during the CV experiment is controlled by slow kinetics due to sluggish electron transfer (irreversible reactions). The ratio of anodic to cathodic peak currents is ($I_{pa}/I_{pc} \neq 1$), and the distance between peak potentials (ΔE_p) is > 0.059 V/n.[21,22] Typically, when a chemical reaction precedes or succeeds a redox process, the ratio of I_{pa}/I_{pc} is less than 1, and the voltammogram exhibits a smaller reverse peak because the product is chemically removed from the surface, and there is a shift in peak potential with scan rate.[13] Kinetic results are tabulated in Table III.

It is seen from the results, that as scan rate increases from 5 to 25 mV s^{-1}, the anodic and cathodic peaks are reduced in size and become widely separated with the reverse peaks smaller than the forward peaks. Well-defined redox peaks are caused by the formation of a diffusion layer near the electrode surface, which increases at higher scan rates than at lower scan rates.[11] A gradual increase in anodic and cathodic peak current is observed with increasing number of cycles indicative of a progressive adsorptive accumulation at the surface. Kinetic data show that increasing scan rate increases peak separation distance (ΔE_p) (>0.059 V/n) suggesting strong irreversibility, which does not follow the Nernstian behavior. The dependence of peak potential on the scan rate for an irreversible reaction characterized by shifts in peak potential with increasing scan rate is expressed in eq. (2):

Table I. FTIR Peak Assignments for Neat Polyimide and Graphene/Polyimide System

Peak assignment	Neat polyimide (wavenumbers in cm^{-1})	Graphene/polyimide (wavenumbers in cm^{-1})
Asymmetric stretching of C=O imide bond	1,778	1,774
Symmetric stretching of C=O imide bond	1,714	1,716
Stretching of aromatic ring	1,496	1,496
C—N—C bond stretching	1,370	1,370
C—O bond bending	719	719

$$E_p = E^o - \frac{RT}{\alpha nF}\left[0.78 - \ln\frac{k^O}{D^{\frac{1}{2}}} + \ln\left(\frac{\alpha nFv}{RT}\right)^{\frac{1}{2}}\right] \quad (2)$$

where, α is the transfer coefficient, n is the number of electrons, D is the diffusion coefficient, v is the scan rate, and E^0 is the standard potential. The effect of scan rate on the peak current

Table II. EOI of Graphene/Polyimide System at Different Curing Temperatures for 1 h

Curing temperature (°C)	Extent of imidization (EOI) (%)
120	14
200	52
250	79

for a totally irreversible systems can be expressed as shown in eq. (3):

$$i_p = (2.99x10^5)n(\alpha n)^{\frac{1}{2}}ACD^{\frac{1}{2}}v^{\frac{1}{2}} \quad (3)$$

Equations (2) and (3) are used to estimate the reaction rate constant and diffusion coefficient. When the CV of the composites was carried out using KPF_6-NMP electrolyte–solvent system at a scan rate of 50 mV s^{-1} and a potential range of −0.2 to 0.8 V, no redox peaks was observed in the voltammogram as shown in Figure 5(d); however, a cyclic curve with rounded corners is seen. Polarization of charges occur on the material's surface where negative ions are accumulated on the cathode and positive ions at the anode with no electron transfer.[23] Separation of charges at the electrode/electrolyte solution interface

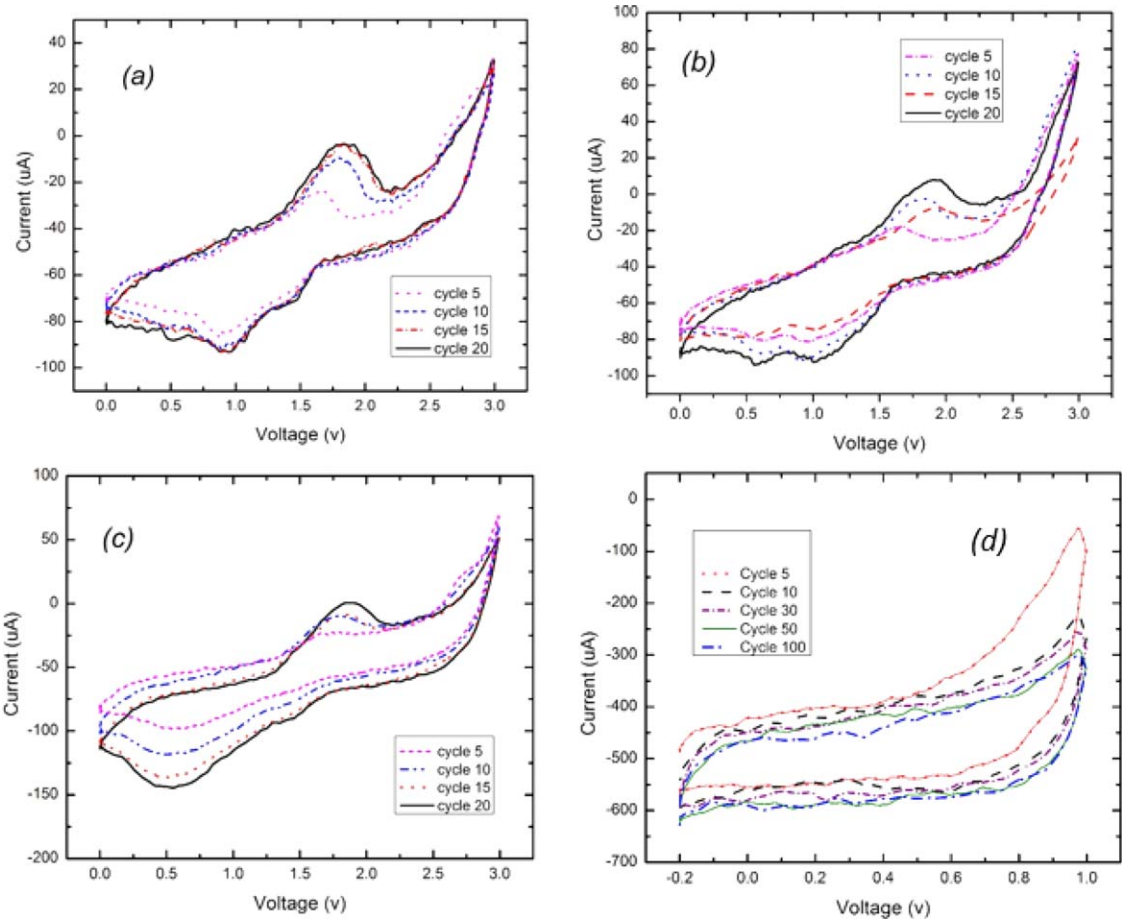

Figure 5. Cyclic voltammograms at scan rates of (a) 5 mV s^{-1}, (b) 15 mV s^{-1}, and (c) 25 mV s^{-1} using KPF6-PC electrolyte solution and (d) at scan rate of 50 mV s^{-1} using KPF6-NMP electrolyte solution. [Color figure can be viewed in the online issue, which is available at wileyonlinelibrary.com.]

Table III. Kinetics Data Obtained from CV Experiment Using KF6-PC Electrolyte System

	Scan rate					
	5 mV s^{-1}		15 mV s^{-1}		25 mV s^{-1}	
Cycles	ΔE_p (V)	I_{pa}/I_{pc}	ΔE_p (V)	I_{pa}/I_{pc}	ΔE_p (V)	I_{pa}/I_{pc}
5	0.8046	0.2621	0.7727	0.5348	1.0841	0.1938
10	0.9122	0.1032	0.6585	0.4000	1.3239	0.0729
15	0.9587	0.0341	1.5092	0.0853	1.3389	0.0638
20	0.9222	0.0384	1.3953	0.0864	1.3045	0.0382

leads to the formation of an electric double layer where charge is stored. Ions are drawn to the electric double layer during voltage scans and charged, producing current in the process and when the scan is reversed, it is discharged. Materials which exhibit this type of electric double layer behavior are highly desirable for use as supercapacitors. The observed difference in the behavior of the composites in the two different electrolyte–solvent systems is said to be due to the coordination of solvent molecules to electrolyte ions; NMP solvent molecules tend to form a hard solvation sheath around the electrolyte ion, thereby decreasing its mobility and reactivity unlike PC which mildly solvates the ions.[13] A plot of specific capacitance vs. number of cycles is shown in Figure 6(a,b) and indicates attainment of stability after 20 cycles. Specific capacitance is higher at lower scan rates because lower scan rates allows adequate time for charging of electric double layer or charge transfer before the potential is switched. Specific capacitance values obtained using both electrolyte solutions are comparable. CV measurements demonstrate the dual behavior of the composite film exhibiting both pseudo-capacitance and electric double layer capacitance depending on the solvent used.

Figure 7(a,b) shows the Bode and Nyquist plots obtained from EIS experiment. Bode plot shows higher impedance values for the films when tested in KPF_6-NMP electrolyte solution compared with KPF_6-PC electrolyte solution. This is attributed to a hard solvation of electrolyte ions in NMP solvent, which leads to increased diffusion resistance due to larger radius of solvated ions.[13,24,25] The Nyquist plot shows a Warburg impedance at the low frequency region consistent with diffusion through a porous electrode. The slope of the Warburg line represents ion diffusion resistance in the porous electrode.[26] At the high frequency region (>1 kHz), the material exhibits a purely resistive behavior, and at intermediate to low frequency regions, it exhibits both capacitive and resistive behavior due to penetration of electrolyte ions through the bulk of the electrode. The continuous increase in the imaginary impedance at low frequency region represents a purely capacitive behavior due to ion adsorption on the electrode surface. Both electrolyte solutions show deviation from the vertical 90° ideal capacitive behavior, and the extent of deviation is given by eq. (4):

$$Z'' = \frac{1}{(jCW)^{\alpha}} \Rightarrow \log(Z'') = -\alpha \times \log(Cw) \quad (4)$$

where, $0 < \alpha < 1$. α can be extracted by plotting a graph of the imaginary impedance versus log of frequency.[27] A transmission line model [Figure 7(c)] consisting of a Warburg element (W_d), resistors, and capacitors in series is used to fit data from the Nyquist plot. Fitted data show bulk resistance of 0.89 and 3.45

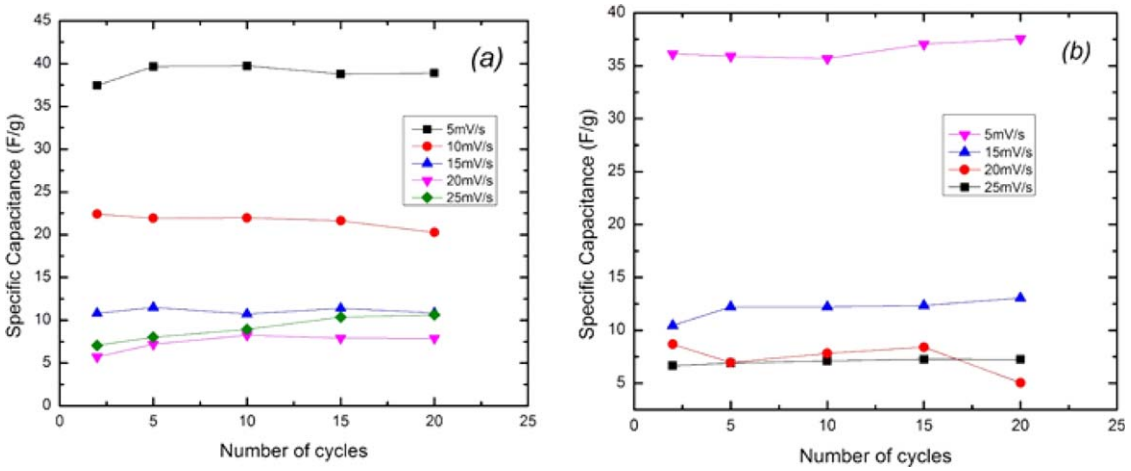

Figure 6. Plot of specific capacitance vs. no. of cycles for (a) system tested with KPF_6-PC electrolyte and (b) system tested with KPF_6-NMP electrolyte solution. [Color figure can be viewed in the online issue, which is available at wileyonlinelibrary.com.]

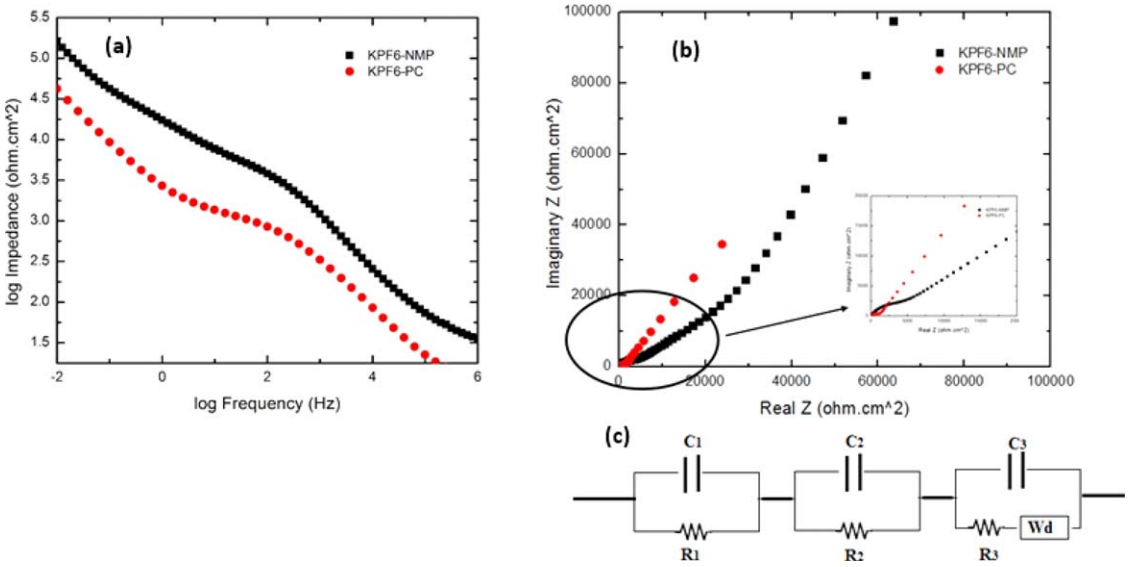

Figure 7. (a) Bode plots, (b) Nyquist plots, and (c) transmission line model used for fitting Nyquist plots for graphene/polyimide composite system in KPF6-PC and KPF6-NMP electrolyte solutions. [Color figure can be viewed in the online issue, which is available at wileyonlinelibrary.com.]

kohm and α values of 0.66 and 0.54 for the films when tested in KPF_6-PC and KPF_6-NMP electrolyte solutions, respectively. A modified form of Archie's law is theoretically used to calculate composite film's porosity using bulk resistance values obtained from EIS studies. Effective ionic conductivity (σ_{eff}) is calculated using eq. (5).[28]

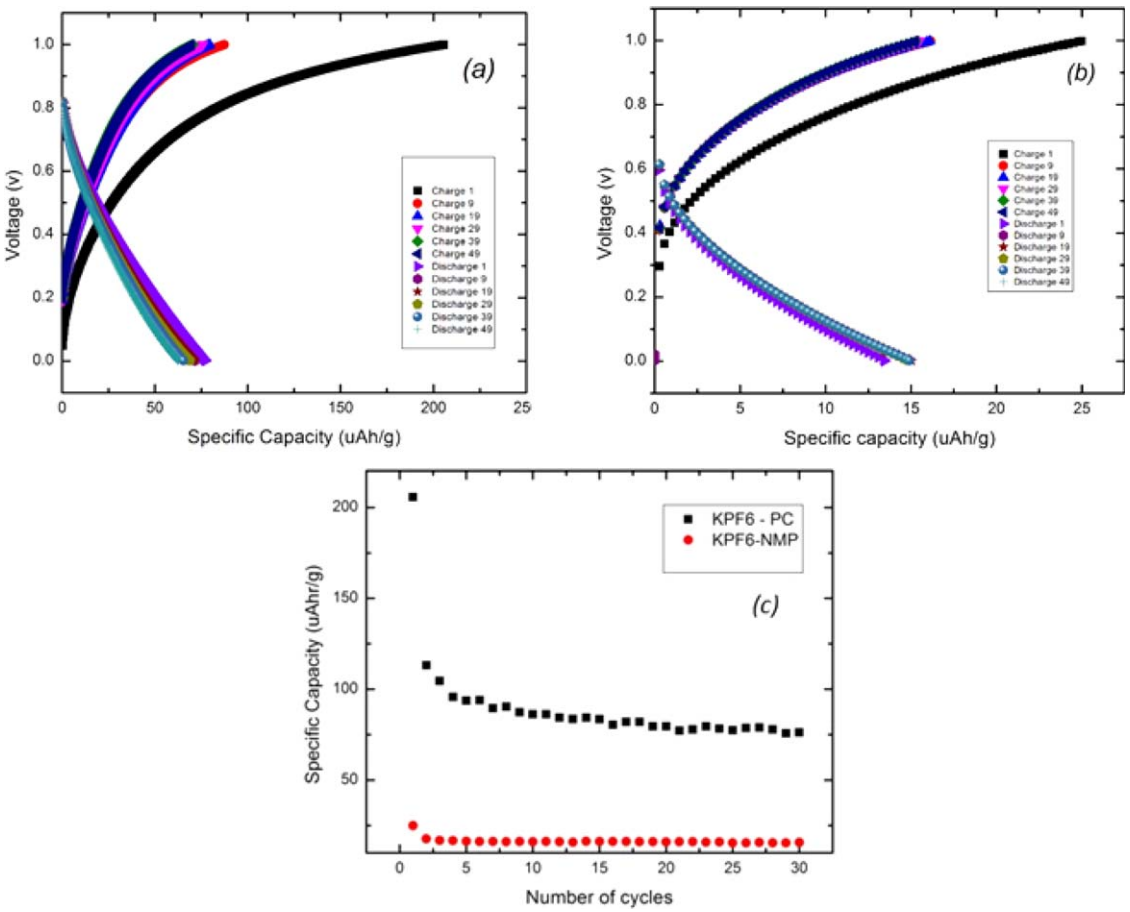

Figure 8. Plot of voltage versus specific capacity for (a) KPF_6-PC and (b) KPF_6-NMP electrolyte solution for 50 cycles. (c) Plot of specific capacity versus number of cycles. [Color figure can be viewed in the online issue, which is available at wileyonlinelibrary.com.]

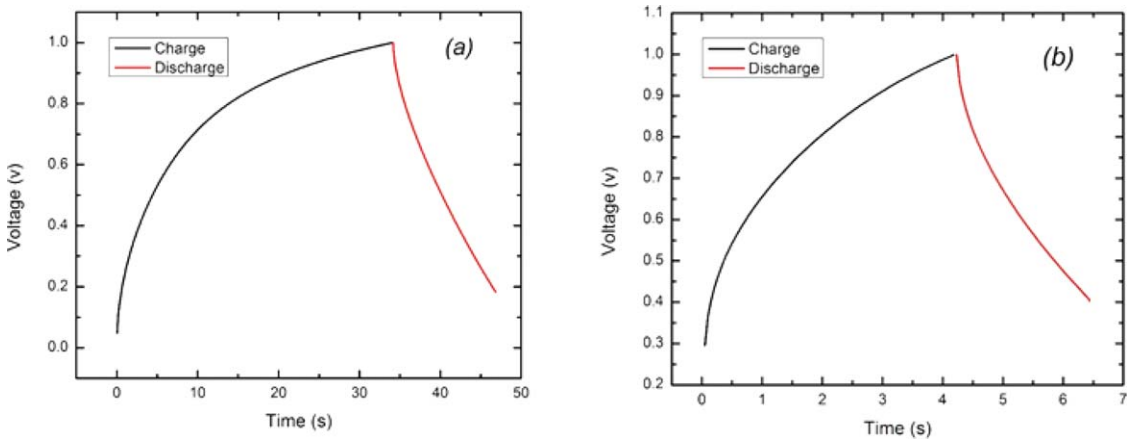

Figure 9. Plot of voltage versus time for (a) KPF_6-PC and (b) KPF_6-NMP electrolyte solution for first cycle. [Color figure can be viewed in the online issue, which is available at wileyonlinelibrary.com.]

$$\sigma_{\text{eff}} = \frac{t}{R_b A} \tag{5}$$

where, R_b is the materials bulk resistance, t is thickness of the sample, and A is the contact area of electrode material. The pore volume/porosity ($\varnothing_0$) is then related to the effective conductivity by:

$$\varnothing_o = \sqrt[m]{\frac{\sigma_{\text{eff}}}{C\sigma_o}} \tag{6}$$

where σ_0 is the conductivity of the electrolyte solution, which is 6.4 mS cm^{-1} for PC at 20°C,[29] C is the coefficient of saturation ranging from 0.1 to 1, and m is the cementation factor typically in the range of 1.5–4. Calculated theoretical porosity is about 10%. Low porosity is due to the stiffening effect of hard graphene fillers in polyimide matrix resulting in a very rigid material with restricted pores. The material's bulk resistance can be improved by improving the material's porosity, thereby providing a better pathway for ion diffusion.

Figure 8(a,b) shows CCD curves for the composites. A significant drop in specific capacity and a shift in working voltage to lower values after the first cycle are observed due to ohmic (IR) drop. When the composite is tested in KPF_6-NMP electrolyte solution, the composite exhibits higher IR drops due to its high bulk resistance value (~3.45 kohm). In KPF_6-PC electrolyte solution, ohmic loss is lower due to the lower bulk resistance (~0.89 kohm). Figure 8(c) shows relatively lower specific capacity values for the material when tested in KPF_6-NMP than in KPF_6-PC electrolyte solution. This is said to be due to the nature of the solid electrolyte interface (SEI) formed on the material's surface during charging. The SEI stabilizes output capacity and improves cycle stability. In a recent study, Wang and Yoshio[24] investigated the nature of SEI formed on an activated carbon/graphite electrode when tested in different electrolyte solutions. They showed that SEI formed with KPF_6-PC electrolyte solution is less dense and thin due to the mild solvation of potassium ions in PC, which allows for easy passage of naked potassium ions through the film and into the material bulk contributing to higher capacity. On the other hand, the hard solvation of electrolyte ions in NMP prevents bound solvated-potassium ions from stripping free from solvent molecules and migrating to inner regions of the material resulting in lower output capacity. Figure 9(a,b) shows charge/discharge versus time plots for both electrolyte systems after the first cycle. Very short charge and discharge time is observed in KPF_6-NMP electrolyte solution due to poor accessibility of electrolyte ions through the material's bulk. However, with KPF_6-PC electrolyte, a longer charging time is observed because of ease of migration of bare potassium ions through the micropores of the material, resulting in higher capacity. The nonlinear shape of the curves is due to ohmic losses. Output power, p, is calculated by using eq. (7): p is inversely related to resistance.

$$P = \frac{U^2}{4R_s} \tag{7}$$

where U is voltage and R_s is the series resistance (ESR).[16,30,31] Output power for the system are 281 and 72.5 μW when tested in KPF_6-PC and KPF_6-NMP electrolytes solutions, respectively. High bulk resistance has negative impact on output power as shown in the results. The composites power density can be improved by sufficiently improving their bulk resistance.

CONCLUSION

Electrochemical behavior of graphene/polyimide composite is investigated using two different electrolyte solutions. The focus of the study is on a grapheme/polyimide composites containing 50 wt % of graphene. In general, better electrochemical behavior was obtained for the composites when they were tested in KPF_6-PC electrolyte–solvent system compared with KPF_6-NMP electrolyte–solvent system because of better electrolyte ion–solvent dipole interaction in the former. CV results show that the composite material supports both redox reactions and allows polarization of charges in its electric double layer. This dual behavior makes it a highly desirable electrode material for energy storage. Significant power losses are observed because of the material's high internal resistance, which can be reduced by increasing the material's porosity and available areas for ion adsorption. Further work is being done to improve the material's architecture and enhance electrochemical properties.

ACKNOWLEDGMENTS

Thanks to Elsiever for granting us permission to publish Figures 2a and b.

REFERENCES

1. Huggins, R. A. *Solid State Ionics* **2000**, *134*, 179.
2. Imjee, F. I.; Chou, P. H. Everlast: Long-life Supercapacitor-operated Wireless Sensor Node, In: Proceedings of International Symposium on Low Power Electronics and Design, Tegernsee; Bavaria, Germany, *2006*.
3. Kotz, R.; Carlen, M. *Electrochim. Acta* **2000**, *45*, 15.
4. Das, T. K.; Prusty, S. *Polym. Plast. Technol. Eng.* **2013**, *52*, 319.
5. Peng, C.; Zhang, S.; Jewell, D.; Chen, G. Z. *Prog. Nat. Sci.* **2008**, *18*, 777.
6. Longun, J.; Iroh, J. O. *Carbon* **2012**, *50*, 1823.
7. Lee, H.; Kang, J.; Cho, M. S.; Choi, J. B.; Lee, Y. *J. Mater. Chem.* **2008**, *21*, 18215.
8. Pasahan, A. In High Performance Polymers – Polyimides Based – From Chemistry to Applications; Abadi, M. J. M., Ed.; Intech PrePress: Novi Sad, Serbia, **2012**; Chapter 10, pp 199–211.
9. Jo, G.; Choe, M.; Lee, S.; Park, W.; Kahng, Y. H.; Lee, T. *Nanotechnology* **2012**, *23*, 112001.
10. Nicholson, R. S. *Anal. Chem.* **1965**, *37*, 1351.
11. Yoonessi, M.; Shi, Y.; Scheiman, D. A.; Lebron-Colon, M.; Tigelaar, D. M.; Weiss, R. A.; Meador, M. A. *ACS Nano* **2012**, *6*, 7644.
12. Kim, G. Y.; Choi, M.-C.; Lee, D.; Ha, C.-S. *Macromol. J.* **2012**, *297*, 303.
13. Reiger, P. H. Electrochemistry, 2nd ed.; Chapman & Hall: New York, **1994**.
14. Xu, K. *Chem. Rev.* **2004**, *104*, 4303.
15. Wang, Y.; Shi, Z.; Fang, J.; Xue, H.; Ma, X.; Yin, J. *J. Mater. Chem.* **2011**, *21*, 505.
16. Calizo, I.; Balandin, A. A.; Bao, W.; Miao, F.; Lau, C. N. *Nano Lett.* **2007**, *7*, 2645.
17. Hodkiewicz, J. Characterizing Graphene with Raman Spectroscopy; Thermo Fisher Scientific, Madison, WI, Appl. Note: 51946.
18. Tang, Z.; Zhang, L.; Zeng, C.; Lin, T.; Guo, B. *Soft Matter* **2012**, *8*, 9214.
19. Childres, I.; Jauregui, L. A.; Park, W.; Cao, H.; Chen, Y. P. In New Developments in Photon and Materials Research; Jang, J. I., Ed.; Nova Scientific Publishers: New York, **2013**; Chapter 19.
20. Wang, J.; Iroh, J. O.; Long, A. *J. Appl. Polym. Sci.* **2012**, *125*, E486.
21. Bard, A. J.; Faulkner, L. R. Electrochemical Methods: Fundamentals and Applications, 2nd ed.; John Wiley: New York, **2001**.
22. Wang, J. Analytical Electrochemistry, 2nd ed.; Wiley-VCH: New York, **2000**; Chapter 2, p 28.
23. Pieta, P.; Obraztsov, I.; D'Souza, F.; Kutner, W. *ECS J. Solid State Sci. Technol.* **2013**, *2*, M3120.
24. Wang, H.; Yoshio, M. *J. Power Sources* **2010**, *195*, 1263.
25. Izutsu, K. Electrochemistry in Nonaqueous Solutions, 2nd ed.; Wiley-VCH: Weinheim, Germany, **2009**.
26. Dolah, B. N. M.; Othman, M. A. R.; Deraman, M.; Basri, N. H.; Farma, R.; Talib, I. A.; Ishak, M. M. *J. Phys.: Conference Series* **2013**, *431*, 012015.
27. Segalini, J.; Daffos, B.; Taberna, P.-L.; Gogotsi, Y.; Simon, P. *Electrochim. Acta* **2010**, *55*, 7489.
28. Tully-Dartez, S.; Cardenas, H. E.; Sit, P.-F. S. *Tissue Eng. Part C* **2010**, *16*, 339.
29. Herlem, G.; Fahys, B.; Herlem, M.; Penneau, J.-F. *J. Sol. Chem.* **1999**, *28*, 223.
30. Liu, C.-Y.; He, J.; Keunings, R.; Bailly, C. *Macromolecules* **2006**, *39*, 8867.
31. Bruce, P. G.; Scrosati, B.; Tarascon, J. M. *Angew. Chem. Int. Ed.* **2008**, *47*, 2930.